Japanese Journal of Applied Physics
Vol. 47, No. 7, 2008, pp. 5516–5520

Electronic Band Structure and Optical Properties of $Sr_{n+1}Ti_nO_{3n+1}$ Ruddlesden–Popper Homologous Series

Ali Hussain RESHAK*, Sushil AULUCK[1], and Ivan KITYK[2]

Institute of Physical Biology, South Bohemia University, Institute of System Biology and Ecology, Academy of Sciences, Nove Hrady 37333, Czech Republic
[1]*Physics Department, Indian Institute of Technology, Kanpur (UP) 208016, India*
[2]*Institute of Chemistry, Silesian Thechnological University, ul. Strzody 9, Gliwice, Poland*

(Received December 21, 2007; revised February 8, 2008; accepted February 12, 2008; published online July 11, 2008)

State-of-the-art calculations of electronic band structures, density of states and frequency-dependent optical properties have been reported for $Sr_{n+1}Ti_nO_{3n+1}$ ($n = 1, 2, 3, \infty$) compounds. These materials possess indirect wide energy band gaps. The frequency dependent optical properties of $n = 1, 2, 3$ compounds show considerable anisotropy and positive birefringence. The conduction band minimum is originates from Ti-d states, while the valence band maximum is governed by O-p states. The bandwidth of the Ti-d states is responsible for the decrease in the energy band gap as n changes from 1 to 2, 3, and ∞. We have analyzed the degree of hybridization on the basis of the ratio of the orbital overlapping within the muffin tin sphere.
[DOI: 10.1143/JJAP.47.5516]

KEYWORDS: electronic structure, optical properties, DFT, LDA, FPLAPW

1. Introduction

Among the oxide materials, $Sr_{n+1}Ti_nO_{3n+1}$ ($n = 1, 2, 3, \infty$) is of special interest owing to its superior dielectric properties,[1] the chemical and structural stability in a wide temperature range.[2,3] These materials have attracted considerable interest because they show various promising physical properties.[4–9] The investigated compounds can be used as dielectric materials in capacitors, infrared detectors, oxygen ion conductors in sensors, substrates for high T_c superconductors, or as piezoelectric materials in actuators.[10–15] They have wide energy band gaps.[4] $Sr_{n+1}Ti_nO_{3n+1}$ compounds exhibit a wide range of electrical behavior varying from a high-dielectric-constant paraelectric in its undoped form to a superconductor when doped with a variety of elements.[16] It has been studied as a substrate for perovskite oxides and is used in tunable dielectric devices,[17,18] dynamic random access memory, and as an alternative gate oxide in metal–oxide–semiconductor field-effect transistors.[19] Noguera[20] carried out a theoretical study of the atomic and electronic structures of the Sr_2TiO_4, $Sr_3Ti_2O_7$, $Sr_4Ti_3O_{10}$, and $SrTiO_3$ compounds, using the total-energy semiempirical Hartree–Fock method. He found that these compounds become more unstable with respect to phase dissociation. Haeni *et al.*[21] grew the first five members of the $Sr_{n+1}Ti_nO_{3n+1}$. They confirmed that these films are epitaxially oriented and nearly free of intergrowths as determined from X-ray diffraction and high-resolution transmission electron microscopy images. Wise *et al.*[22] measured the X-ray diffraction, transmission electron microscopy, and microwave dielectric properties of the $(Sr_xCa_{(1-x)})_{n+1}Ti_nO_{3n+1}$ series. Hungria *et al.*[23] presented a new method of synthesis, mechanochemical activation, for the preparation of the $Sr_3Ti_2O_7$ phase. Kamba *et al.*[24] studied the room-temperature infrared reflectivities, time domain THz transmission spectra and micro-Raman spectra of ceramics in the Ruddlesden–Popper homologous series $Sr_{n+1}Ti_nO_{3n+1}$ ($n = 1, 2, 3, 4, \infty$). Fennie and Rabe[25] investigated the structural and dielectric properties of Sr_2TiO_4 within the density functional theory (DFT). Inaguma *et al.*[26] prepared and investigated the photoluminescence properties of the perovskite-related compounds $Sr_{n+1}Ti_nO_{3n+1}:Pr^{3+}$ ($n = 1, 2, \infty$) by a Pechini-type polymerizable complex method. Matsuno *et al.*[27] synthesized single-crystalline thin films of layered Sr_2MO_4 (M = Ti, V, Cr, Mn, and Co) and studied the variation of the electronic structure. Weng *et al.*[28] investigated the electronic structure and optical conductivity spectra of a series of layered perovskites, Sr_2MO_4 (M = Ti, V, Cr, Mn, and Co), using *ab initio* calculation with generalized gradient approximation (GGA) and GGA+U method. They found that the GGA calculation could successfully predict the ground states of M = Ti, Mn, and Co, but failed in the case of M = V and Cr. For the strongly correlated t_{2g} system, GGA+U could give the most stable state, being the antiferromagnetic (AFM-II) configuration as suggested from the experimental measurements. Gutmann *et al.*[29] prepared thin films of perovskite-related $Sr_{n+1}Ti_nO_{3n+1}$ Ruddlesden–Popper phases ($n = 1, 2, 3$), which were grown oriented on (001) single-crystalline $SrTiO_3$ substrates via wet chemical deposition from Sr-rich metalorganic Sr–Ti solutions and subsequent annealing in air atmosphere at a maximum temperature of 700 °C. The films were investigated by wide-angle X-ray scattering and high-resolution transmission electron microscopy.

From the above, we note that there is dearth of theoretical calculations for the electronic band structure and optical properties. However, no full-potential calculations exist for these compounds. In this current work, we will present a quantitative study on these interesting semiconductor compounds, which is based on the full-potential (FP) method. The more general treatment of the potential, such as provided by the FP method has none of the drawbacks of the methods based on the atomic sphere approximation (ASA) and muffin-tin approximation (MTA). In the FP methods, the potential and charge density are expanded into lattice harmonics inside each atomic sphere and as a Fourier series in the interstitial region. We therefore consider it useful to perform *ab initio* calculations for these compounds. In this present work, we use the full-potential linear-

*E-mail address: maalidph@yahoo.co.uk

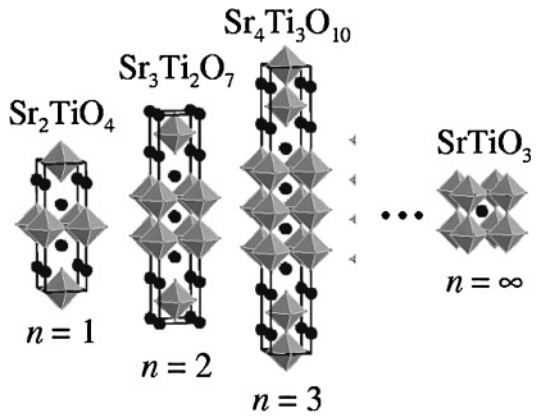

Fig. 1. Structure of $Sr_{n+1}Ti_nO_{3n+1}$ unit cell of RP homologous series. Circles represent the Sr atoms: Ti atoms are at the centers of the octahedra with the oxygen atoms.

augmented plane wave (FP-LAPW) method, which has proven to be one of the most accurate methods[30,31] for the computation of the electronic structure of solids within the DFT. Hence, the effect of the FP on the electronic band structure, density of states and linear optical properties can be ascertained.

2. Structural Aspects and Computational Details

$Sr_{n+1}Ti_nO_{3n+1}$ $(n = 1, 2, 3, \infty)$ Ruddlesden–Popper compounds have the general formula $A_{n+1}B_nO_{3n+1}$ and are composed of n perovskite blocks separated and sheared by rock-salt-structured layers along (1/2)(111) (Fig. 1). The $(n = 1, 2, 3)$ compounds belong to the tetragonal structure with space group $I4/mmm$ (no. 139), while the $(n = \infty)$ compound belongs to the cubic structure with the space group $Pm3m$.[32] The experimental lattice parameters[22] are listed in Table I.

In our calculations, we use the state-of-the-art FPLAPW method in a scalar relativistic version as embodied in the WIEN2K code.[33] This is an implementation of the DFT with different possible approximations for the exchange correlation (XC) potential. XC is treated within the local density approximation (LDA),[34] and scalar relativistic equations are used to obtain self-consistency. The Kohn–Sham equations are solved using a basis of linear APW's.

To achieve energy the convergence of eigenvalues, the wave functions in the interstitial region were expanded in plane waves with a cut-off $K_{\max} = 7/R_{\mathrm{MT}}$, where R_{MT} denotes the smallest atomic sphere radius and $K_{\max}$ represents the magnitude of the largest K vector in the plane wave expansion. The R_{MT} values are 2.0, 1.8, and 1.4 atomic units (a.u.) for Sr, Ti, and O, respectively, for $n = 1$ and 2, while they are 2.4, 1.85, 1.64 a.u. for $n = 3$, and 2.5, 1.94, 1.72 a.u. for $n = \infty$. The valence wave functions inside the spheres are expanded up to $l_{\max} = 10$ while the charge density was Fourier expanded up to $G_{\max} = 14$. Self-consistency is achieved using 170 $\boldsymbol{k}$ points in the irreducible Brillouin zone (IBZ). We calculated the frequency-dependent linear optical properties using 500 $\boldsymbol{k}$ points in the IBZ.

Table I. Lattice parameters and atomic positions for $Sr_{n+1}Ti_nO_{3n+1}$.

$Sr_{n+1}Ti_nO_{3n+1}$	a (Å)	c (Å)	Sr	Ti	O
$n = 1$	3.88	12.6	(0, 0, 0.648)	(0, 0, 0)	(0, 0.5, 0), (0, 0, 0.849)
$n = 2$	3.90	20.38	(0, 0, 0.5), (0, 0, 0.312)	(0, 0, 0.094)	(0, 0, 0) (0, 0.5, 0.094) (0, 0, 0.188)
$n = 3$	3.90	28.1	(0, 0, 0.431) (0, 0, 0.295)	(0, 0, 0) (0, 0, 0.134)	(0, 0.5, 0) (0, 0, 0.068) (0, 0.5, 0.136) (0, 0, 0.204)
$n = \infty$	3.89		(0, 0, 0)	(0.5, 0.5, 0.5)	(0, 0.5, 0.5)

3. Results and Discussion

3.1 *Band structure and density of states*

Figures 2 and 3 show the self-consistent electronic band structure and total density of states (TDOS) along with the Sr-s/p/d, Ti-s/p/d, and O-s/p partial (PDOS) for the $Sr_{n+1}Ti_nO_{3n+1}$ $(n = 1, 2, 3, \infty)$ compounds. For the $n = 1, 2, 3$ compounds, the valence band maximum (VBM) is located at X, whereas it is located at M for $n = \infty$. The conduction band minimum (CBM) is located at Γ for all compounds resulting in an indirect energy gaps of 1.93, 1.85, 1.79, and 1.71 eV for $n = 1, 2, 3, \infty$, respectively. We note that the energy gap decreases when we move from $n = 1$ to 2, 3, and ∞. This could be attributed to the fact that the conduction band minimum has strong cation-d states while the other states in the conduction band are more heavily mixed with the atomic orbitals such as anion-s states. In the conduction bands, shifting the anion-s states has a small effect whereas shifting the cation-d states has a strong effect in opening the gap, while leaving the valence bands unchanged. Hence, the conduction bands shift towards the Fermi energy (E_{F}) when we go from $n = 1$ to 2 to 3 to ∞. The overall decrease in the band gap is consistent with an overall weakening of the bonds and, therefore, with a smaller bonding anti-bonding splitting. The calculated energy gaps are smaller than the experimental gaps (3.25–3.5 eV)[36,37] as expected from an LDA calculation.[35] LDA calculations underestimate the band gaps by approximately 30–40%. When this is considered and if we allow for structural relaxations, this above-mentioned trend could change.

The band structure and, hence, the density of states (DOS) can be divided into four groups/structures. From the PDOS, we can to identify the angular momentum character of the various structures. The lowest energy groups (first and second groups) have significant contributions from O-s and Sr-p states with a small contribution from Ti-s/p. The third group between −4.8 eV up to the Fermi energy (E_{F}) is mainly due to the O-p and Ti-p states with insignificant contribution from the O-s and Sr-p states. The last group from the conduction band minimum and above has contributions from the Ti-d and Sr-d states with a small contribution from O-p states. We note the following points: (1) all the O-p characters are concentrated in the upper valence band, with only small amounts in the conduction band, (2) all the Ti-d characters are concentrated in the lower conduction band, with only small amounts in the valence band, and (3) all the Sr-d characters are concentrated in the upper conduction band, with only negligible amounts in the

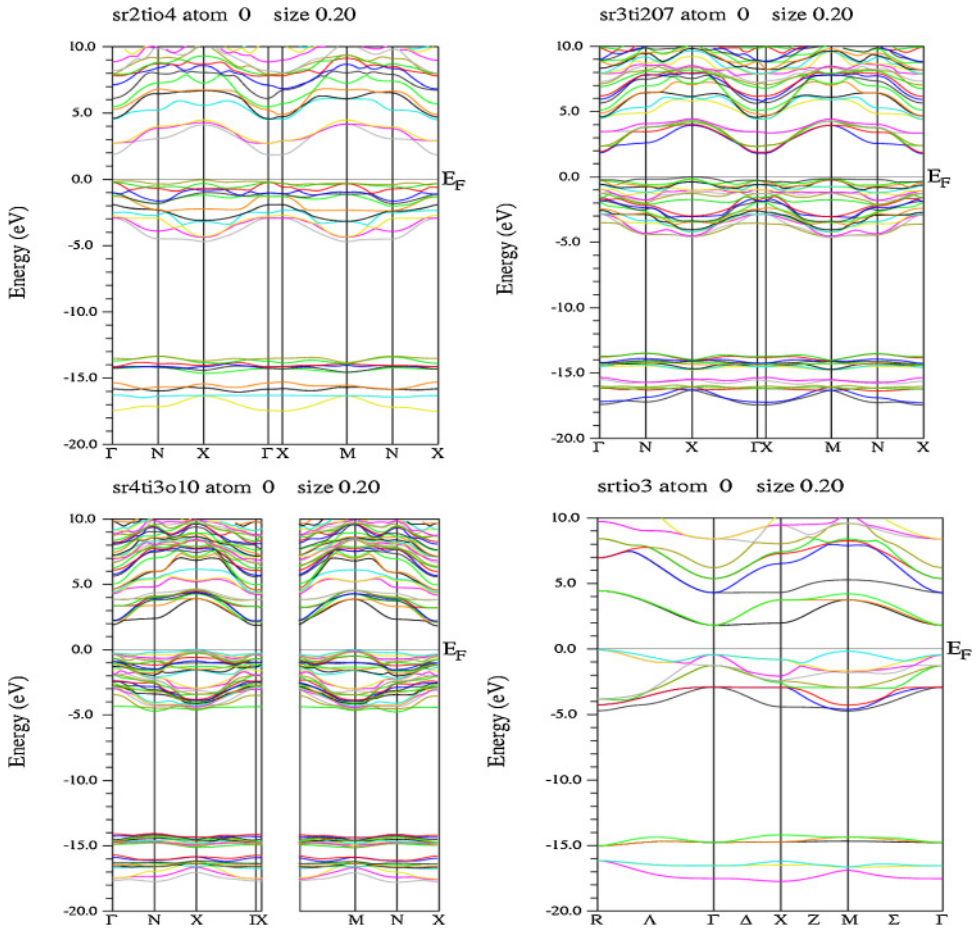

Fig. 2. (Color online) Band structure of $Sr_{n+1}Ti_nO_{3n+1}$ compounds ($n = 1, 2, 3, \infty$).

valence band. The trends in the band structures (as we move from $n = 1$ to 2 to 3 to ∞) can be summarized as follows: (1) The bandwidth of the O-p states in the VBM significantly increases. (2) The bandwidth of Ti-d states in the CBM increases when moving from $n = 1$ to 2 to 3 to ∞, resulting in a reduced band gap.

From the PDOS, we can emphasize that there is a strong/weak hybridization between the states. Following Yamasaki *et al.*[38] we can define the degree of hybridization using the ratio of the hybridized states within the muffin tin sphere. On the basis of this we can say that in the first group there is a strong hybridization between the Sr-p and O-s states, and Ti-s with Sr-s in the energy ranges from -18.5 to -14.0 eV. In the second groups there is a weak hybridization between Sr-p and O-s at approximatly -15.0 eV. In the third groups between -4.5 eV up to E_F, there is a strong hybridization between Ti-s and Sr-s. There is a strong hybridization between O-p and Ti-d in the energy range of -4.5 to -2.0 eV, and a weak hybridization in the energy range of -2.0 eV up to E_F. In the last group, Sr-s is strongly hybridized with Ti-s/p in the CBM. We also note that Sr-d weakly hybridizes with Ti-d in the upper CB.

3.2 *Linear optical response and birefringence*

$Sr_{n+1}Ti_nO_{3n+1}$ ($n = 1, 2, 3$) compounds have tetragonal symmetry and, hence, there are two components of the dielectric tensor, corresponding to electric field $\boldsymbol{E}$ perpendicular and parallel to the c-axis. $\varepsilon_2^{xx}(\omega)$ and $\varepsilon_2^{zz}(\omega)$ are the imaginary parts of these two frequency-dependent components. We have performed calculations of the frequency-dependent dielectric function for these compounds using the following expressions:[39,40]

$$\varepsilon_2^{zz}(\omega) = \frac{12}{m\omega^2}\int_{\mathrm{BZ}}\sum\frac{|P^Z_{nn'}(k)|^2\,dS_k}{\nabla\omega_{nn'}(k)}$$

$$\varepsilon_2^{xx}(\omega) = \frac{6}{m\omega^2}\int_{\mathrm{BZ}}\sum\frac{[|P^X_{nn'}(k)|^2 + |P^Y_{nn'}(k)|^2]\,dS_k}{\nabla\omega_{nn'}(k)}.$$

The above expressions are written in atomic units with $e^2 = 1/m = 2$ and $\hbar = 1$. Here, ω is the photon energy and $P^X_{nn}(k)$ is the x component of the dipolar matrix elements between initial $|nk\rangle$ and final $|n'k\rangle$ states with eigenvalues $E_n(k)$ and $E_{n'}(k)$, respectively. $\omega_{nn'}(k)$ is the band energy difference, $\omega_{nn'}(k) = E_n(k) - E_{n'}(k)$, and S_k is a constant energy surface, $S_{k=}[k; \omega_{nn'}(k) = \omega]$.

$Sr_{n+1}Ti_nO_{3n+1}$ ($n = \infty$) has a cubic structure; for calculating the optical properties of the cubic structural material, we need only one dielectric tensor component to completely characterize the linear optical properties. This component is $\varepsilon_2(\omega)$, the imaginary part of the frequency-dependent dielectric function is given as[41]

$$\varepsilon_2(\omega) = \frac{8}{3\pi\omega^2}\sum_{nn'}\int_{\mathrm{BZ}}|P_{nn'}(k)|^2\frac{dS_k}{\nabla\omega_{nn'}(k)},$$

where $P_{nn'}(k)$ denotes the dipolar matrix elements between the initial $|nk\rangle$ and final $|n'k\rangle$ states with their eigenvalues $E_n(k)$ and $E_{n'}(k)$, respectively.

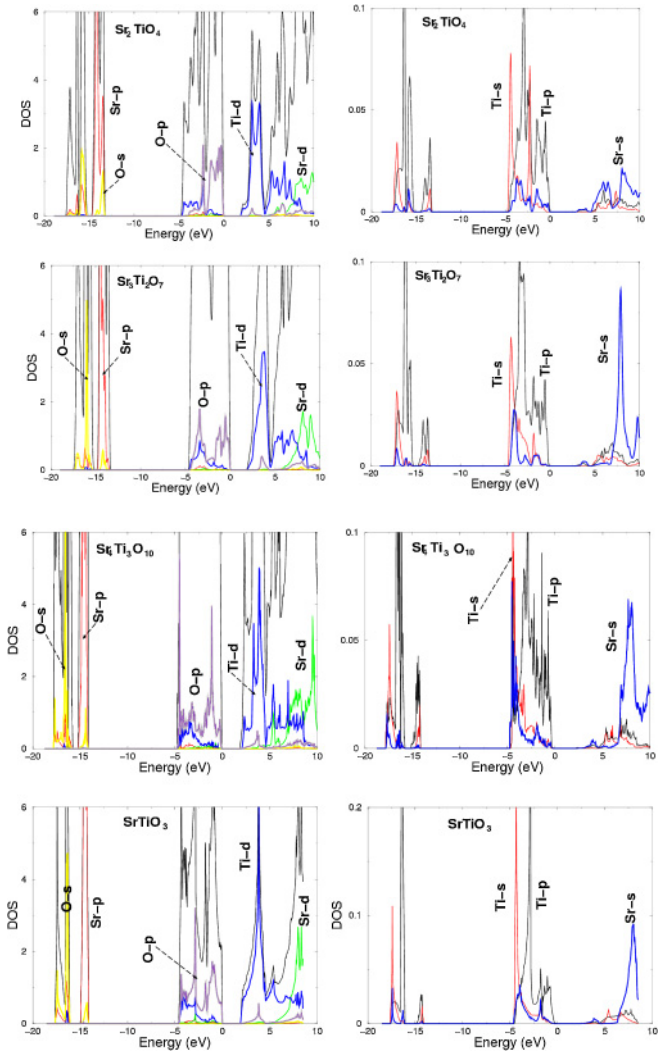

Fig. 3. (Color online) TDOS (states/eV unit cell) along with the Sr-s/p/d, Ti-s/p/d, and O-s/p partial (PDOS) for $Sr_{n+1}Ti_nO_{3n+1}$ ($n = 1, 2, 3, \infty$).

Figure 4 shows the calculated imaginary part of the frequency dependent dielectric function $\varepsilon_2^{xx}(\omega)$, $\varepsilon_2^{zz}(\omega)$, and $\varepsilon_2(\omega)$. A considerable anisotropy is found between $\varepsilon_2^{xx}(\omega)$ and $\varepsilon_2^{zz}(\omega)$. The broadening is considered to be 0.04 eV.

Generally, the peaks in the optical response are determined from the electric-dipole transitions between the valence and conduction bands. Our analysis of $\varepsilon_2^{xx}(\omega)$, $\varepsilon_2^{zz}(\omega)$, and $\varepsilon_2(\omega)$ curves shows that the edge of the optical absorption for $\varepsilon_2(\omega)$ is located at 2.0 eV for $n = \infty$, and $\varepsilon_2^{xx}(\omega)$ and $\varepsilon_2^{zz}(\omega)$ are located at 3.0, 2.6, and 2.4 eV for $n = 1, 2, 3$, respectively. These points correspond to Γ_c–X_v and Γ_c–M_v splitting for $n = 1, 2, 3, \infty$, respectively, which gives the threshold for optical transitions between the VBM and the CBM. This is known as the fundamental absorption edge. Then, it is followed by two main structures. Note that there is a significant hump on the left side of the first structure of $Sr_3Ti_2O_7$. This hump becomes more significant in $Sr_4Ti_3O_{10}$. This is attributed to the increases in the concentrations of Sr, Ti, and O when we move from $n = 1$ to 2 to 3 to ∞. All the $\varepsilon_2^{xx}(\omega)$, $\varepsilon_2^{zz}(\omega)$, and $\varepsilon_2(\omega)$ structures shift toward lower energies when we move from $n = 1$ to 2, 3, and ∞. This is attributed to the increase in the bandwidth of the conduction bands.

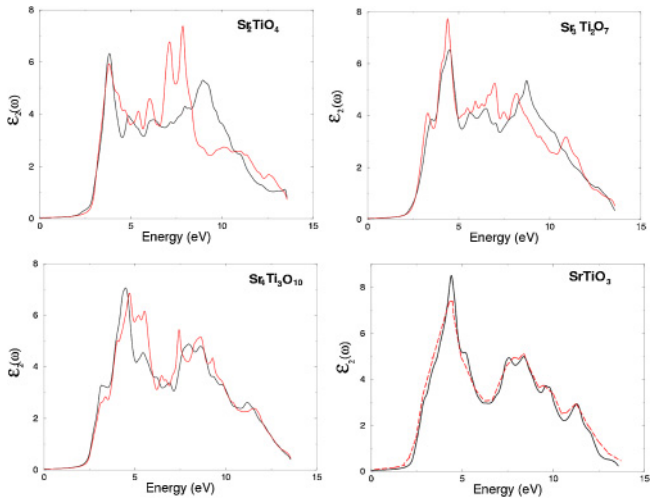

Fig. 4. (Color online) Calculated $\varepsilon_2^{xx}(\omega)$ (dark curve), $\varepsilon_2^{zz}(\omega)$ (light curve), and $\varepsilon_2(\omega)$ for $Sr_{n+1}Ti_nO_{3n+1}$ ($n = 1, 2, 3, \infty$).

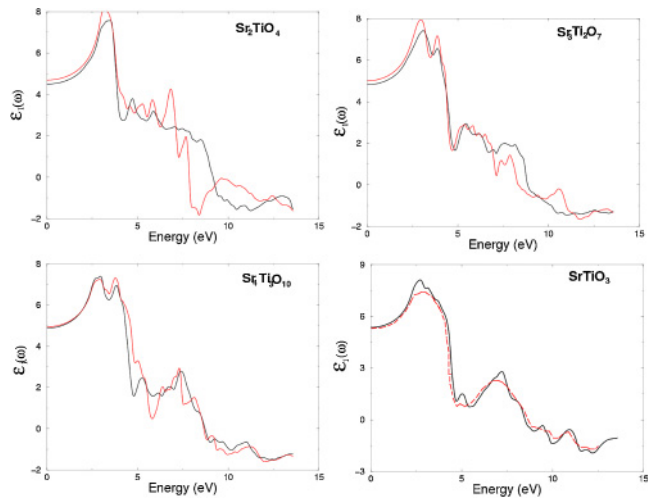

Fig. 5. (Color online) Calculated $\varepsilon_1^{xx}(\omega)$ (dark curve), $\varepsilon_1^{zz}(\omega)$ (light curve), and $\varepsilon_1(\omega)$ for $Sr_{n+1}Ti_nO_{3n+1}$ ($n = 1, 2, 3, \infty$).

Table II. Calculated values of $\Delta n(0)$, $\varepsilon_1^{\perp}(0)$, $\varepsilon_1^{\parallel}(0)$, and $\varepsilon_1^{\text{total}}(0)$ for $Sr_{n+1}Ti_nO_{3n+1}$ ($n = 1, 2, 3$).

$Sr_{n+1}Ti_nO_{3n+1}$	$\Delta n(0)$	$\varepsilon_1^{\perp}(0)$	$\varepsilon_1^{\parallel}(0)$	$\varepsilon_1^{\text{total}}(0)$
$n = 1$	0.024	4.50	4.70	4.57
$n = 2$	0.049	4.82	5.0	4.88
$n = 3$	0.05	4.89	4.95	4.9

From the imaginary part of the dielectric functions, $\varepsilon_2^{xx}(\omega)$, $\varepsilon_2^{zz}(\omega)$, and $\varepsilon_2(\omega)$, the real parts $\varepsilon_1^{xx}(\omega)$, $\varepsilon_1^{zz}(\omega)$, and $\varepsilon_1(\omega)$ are calculated using Kramers–Kronig relations.[42] The results of our calculated $\varepsilon_1^{xx}(\omega)$, $\varepsilon_1^{zz}(\omega)$, and $\varepsilon_1(\omega)$ spectra are shown in Fig. 5. The calculated static value of the dielectric function $\varepsilon_1(0)$ for $n = \infty$ is approximately 5.5, in good agreement with the experimental data.[43] The calculated static values of $\varepsilon_1^{xx}(0)$ and $\varepsilon_1^{zz}(0)$ for $n = 1, 2, 3$ are listed in Table II.

The $Sr_{n+1}Ti_nO_{3n+1}$ ($n = 1, 2, 3$) compounds show considerable anisotropy in the linear optical susceptibilities. The birefringence can be calculated from the linear response functions from which the anisotropy of the index of refraction is obtained. One can determine the value of the extraordinary and ordinary refraction indices. The birefrin-

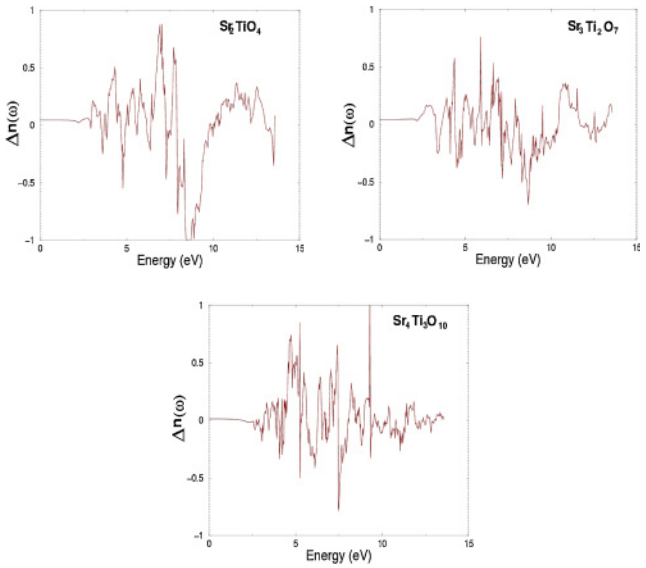

Fig. 6. (Color online) Calculated $\Delta n(\omega)$ for $Sr_{n+1}Ti_nO_{3n+1}$ $(n = 1, 2, 3)$.

gence is the difference between the extraordinary and ordinary refraction indices, $\Delta n = n_e - n_0$, where n_e is the index of refraction for an electric field oriented along the c-axis and n_0 is the index of refraction for an electric field perpendicular to the c-axis. Figure 6 shows the spectral behavior of the birefringence $\Delta n(\omega)$ for $Sr_{n+1}Ti_nO_{3n+1}$. The birefringence is important only in the nonabsorbing region, which is below the energy gap. The $\Delta n(\omega)$ curve shows strong oscillations around zero. These materials possess positive birefringence at zero energy and this is listed in Table II. We are not aware of any experimental data for the birefringence, and we hope that our calculations will lead to such kind of measurements.

4. Conclusions

We have investigated the electronic band structure, density of states and frequency-dependent optical properties of the $Sr_{n+1}Ti_nO_{3n+1}$ $(n = 1, 2, 3, \infty)$ compounds. Our calculations show that these materials possess an indirect wide energy band gap. From the PDOS, we note that the conduction band minimum is governed by Ti-d states, while the valence band maximum is governed by O-p states. The bandwidth of the Ti-d states is responsible for the decrease in the energy band gap while moving from $n = 1$ to 2 to 3 to ∞. We have analyzed the degree of hybridization on the basis of the ratio of the hybridized states within the muffin tin sphere. The frequency-dependent optical properties for $n = 1, 2, 3$ compounds show considerable anisotropy and positive birefringence.

Acknowledgements

This work was supported from the institutional research concept of the Institute of Physical Biology, UFB (No. MSM6007665808) and the Institute of System Biology and Ecology, ASCR (No. AVOZ60870520).

1) E. Hegenbarth: Phys. Status Solidi **6** (1964) 333.
2) T. Nakamura, H. Tokuda, S. Tanaka, and M. Iiyama: Jpn. J. Appl. Phys. **34** (1995) 1906.
3) K. Eisenbeiser, J. M. Finder, Z. Yu, J. Ramdani, J. A. Curless, J. A. Hallmark, R. Droopad, W. J. Ooms, L. Salem, S. Bradshaw, and C. D. Overgaard: Appl. Phys. Lett. **76** (2000) 1324.
4) K. W. Blazey: Phys. Rev. Lett. **27** (1971) 146.
5) H. Fujishita, Y. Shiozaki, and E. Sawaguchi: J. Phys. Soc. Jpn. **46** (1979) 581.
6) M. I. Marques, C. Arago, and J. A. Gonzalo: Phys. Rev. B **72** (2005) 092103.
7) T. Feng: Phys. Rev. B **25** (1982) 627.
8) C. S. Koonce, M. L. Cohen, J. F. Schooley, W. R. Hosler, and E. R. Pfeiffer: Phys. Rev. **163** (1967) 380.
9) D. Kan, R. Kanda, Y. Kanemitsu, Y. Shimakawa, M. Takano, T. Terashima, and A. Ishizumi: Appl. Phys. Lett. **88** (2006) 191916.
10) T. K. Gupta: J. Am. Ceram. Soc. **73** (1990) 1817.
11) V. Ravi Kumar, R. P. Rodrigues, and V. P. Dravid: J. Phys. D **29** (1996) 1799.
12) N. D. Browning, J. P. Buban, H. O. Moltaji, S. J. Pennycook, G. Duscher, U. D. Johnson, P. R. Rodrigues, and V. P. Dravid: Appl. Phys. Lett. **74** (1999) 2638.
13) F. Ernst, O. Kienzle, and M. Ruhle: J. Eur. Ceram. Soc. **19** (1999) 665.
14) D. A. Crandles, B. Nicholas, C. Dreher, C. C. Homes, A. W. McConnell, B. P. Clayman, W. H. Gong, and J. F. Greendan: Phys. Rev. B **59** (1999) 12842.
15) M. Leonhardt, J. Jamnik, and J. Maier: Electrochem. Solid-State Lett. **2** (1999) 333.
16) J. H. Haeni, C. D. Theis, D. G. Schlom, W. Tian, X. Q. Pan, H. Chang, I. Takeuchi, and X.-D. Xiang: Appl. Phys. Lett. **78** (2001) 3292.
17) F. W. Van Keuls, R. R. Romanofsky, D. Y. Bohman, M. D. Winters, and F. A. Miranda: Appl. Phys. Lett. **71** (1997) 3075.
18) X. X. Xi, H.-C. Li, W. Si, A. A. Sirenko, I. A. Akimov, A. M. Clark, and J. Hao: J. Electroceram. **4** (2000) 393.
19) R. A. McKee, F. J. Walker, and M. F. Chisholm: Phys. Rev. Lett. **81** (1998) 3014.
20) C. Noguera: Philos. Mag. Lett. **80** (2000) 173.
21) J. H. Haeni, C. D. Theis, D. G. Schlom, W. Tian, X. Q. Pan, H. Chang, I. Takeuchi, and X.-D. Xiang: Appl. Phys. Lett. **78** (2001) 3292.
22) P. L. Wise, I. M. Reaney, W. E. Lee, T. J. Price, D. M. Iddles, and D. S. Cannell: J. Eur. Ceram. Soc. **21** (2001) 1723.
23) T. Hungria, J. G. Lisoni, and A. Vastro: Chem. Mater. **14** (2002) 1747.
24) S. Kamba, P. Samoukhina, F. Kadlec, J. Pokorny, J. Petzelt, I. M. Reaney, and P. L. Wise: J. Eur. Ceram. Soc. **23** (2003) 2639.
25) C. J. Fennie and K. M. Rabe: Phys. Rev. B **68** (2003) 184111.
26) Y. Inaguma, D. Nagasawa, and T. Katsumata: Jpn. J. Appl. Phys. **44** (2005) 761.
27) J. Matsuno, Y. Okimoto, M. Kawasaki, and Y. Tokura: Phys. Rev. Lett. **95** (2005) 176404.
28) H. Weng, Y. Kawazoe, X. Wan, and J. Dong: Phys. Rev. B **74** (2006) 205112.
29) E. Gutmann, A. A. Levin, M. Reibold, J. Muller, P. Paufler, and D. C. Meyer: J. Solid State Chem. **179** (2006) 1864.
30) S. Gao: Comput. Phys. Commun. **153** (2003) 190.
31) K. Schwarz: J. Solid State Chem. **176** (2003) 319.
32) F. S. Galasso: *Structure and Properties of Inorganic Solids* (Pergamon, Oxford, U.K., 1970) p. 179.
33) P. Blaha, K. Schwarz, G. K. H. Madsen, D. Kvasnicka, and J. Luitz: WIEN2k; An augmented plane wave plus local orbitals program for calculating crystal properties (Vienna University of Technology, Vienna, 2001).
34) W. Kohn and L. J. Sham: Phys. Rev. A **140** (1965) 1133.
35) S. N. Rashkeev and W. R. L. Lambrecht: Phys. Rev. B **63** (2001) 165212.
36) Y. Inaguma, D. Nagasawa, and T. Katsumata: Jpn. J. Appl. Phys. **44** (2005) 761.
37) J. Matsuno, Y. Okimoto, M. Kawasaki, and Y. Tokura: Phys. Rev. Lett. **95** (2005) 176404.
38) T. Yamasaki, N. Suzuki, and K. Motizuki: J. Phys. C **20** (1987) 395.
39) A. Hussain Reshak and S. Auluck: Phys. Rev. B **68** (2003) 245113.
40) S. Sharma, S. Auluck, and M. A. Khan: Pramana—J. Phys. **54** (1999) 431.
41) M. A. Khan, A. Kashyap, A. K. Solanki, T. Nautiyal, and S. Auluck: Phys. Rev. B **48** (1993) 16974.
42) H. Tributsch: Z. Naturforsch. A **32** (1977) 972 [in German].
43) D. Bäuerle, W. Braun, V. Saile, G. Sprüssel, and E. E. Koch: Z. Phys. B **29** (1978) 179 [in German].